Polymer Latex Particle Size Measurement through High Speed Dielectric Spectroscopy

BRYAN B. SAUER,* RUTH S. STOCK,† KYUNG-HEE LIM,‡ and W. HARMON RAY, *Department of Chemical Engineering, University of Wisconsin, Madison, Wisconsin 53706*

Synopsis

Dielectric techniques have been implemented to study aqueous colloidal suspensions. A four-electrode cell was used in two configurations; the first, a sweep of frequencies using a sequence of standard single frequency null-balance measurements, and the second relying on the dielectric response to a Fourier synthesized pseudo random white noise (FSPN) with measurements performed using correlation techniques in the time domain. Single frequency measurements, which take on the order of 5–10 min per spectrum, were performed on polymer latex standards of varying size, latex concentration, and electrolyte concentration and were extended from 0.02 to over 500 kHz. It was found that the central relaxation frequency f_c was inversely proportional to the square of the particle size, consistent with previous experimental results. Experiments were performed at different particle concentrations and ionic strengths, and the magnitude and breadth of the dielectric dispersion was analyzed in terms of current theories. The distribution of relaxation times was found to be in general qualitative agreement with those predicted by some existing theories. The results indicate that a wide range of conditions exist in terms of latex concentration and ionic environment where the rapid and accurate measurement of polymer latex particle size and size distribution is feasible. FSPN measurements, which take on the order of seconds, were shown to be accurate over a moderate frequency range for model electrical network studies but were only partially successful for aqueous suspensions of latex because of high frequency limitations in the electronics. Experimental details and difficulties concerning the application of this technique are discussed.

INTRODUCTION

Technical difficulties have restricted the use of dielectric techniques in polymer latex particle size analysis. The premise of much of the research regarding dielectric relaxation of colloidal particles is that the central relaxation frequency f_c of the dielectric dispersion is dependent on the particle size but independent of both volume fraction and electrolyte concentration over a wide range.[1] The original experiments, which indicated that f_c was dependent on the inverse square of the particle size, were performed on concentrated latex suspensions up to 30% by weight,[1] indicating that the technique is useful at extremely high concentrations where conventional techniques fail. The dielectric relaxation behavior of monomer droplets, dust, and other impurities generally fall out of the frequency range of interest, indicating that the

*Present address: Central R & D Dept., Bldg. 356, Experimental Station, E. I. du Pont de Nemours & Co., Wilmington, DE 19898.

†Present address: Dept. of Chemical Engineering, Wayne State University, Detroit, MI 48202.

‡Present address: Morgantown Energy Technology Ctr., U.S. Dept. of Energy, Morgantown, WV 26507-0880.

Journal of Applied Polymer Science, Vol. 39, 2419–2441 (1990)
 CCC 0021-8995/90/11-122419-23$04.00

technique would have an advantage over other size determination techniques which require dilution, filtration, and various other preparation schemes.

The dielectric experiments of Schwan et al.[1] have raised questions concerning the effect of particle size, double layer thickness, and latex concentration. The study of these has been carried out using conventional techniques such as variable gap methods to compensate for electrode polarization which is detrimental at low frequencies.[2-7] Other methods have been developed with the goal of faster measurements and better ways of avoiding electrode polarization. Differential techniques have been implemented to measure the response of a sample at measurement and reference frequencies[8-12] using four-electrode cells to avoid electrode polarization effects.

An alternate approach to single frequency methods is to use white noise excitation as the input and extract the entire frequency response spectrum from the data. The feasibility of such techniques has been demonstrated,[13,14] indicating that very rapid measurements on nonaqueous polymer solutions are possible. Using a four-electrode cell, Nakamura et al.[15] used a Fourier synthesized pseudo random noise (FSPN) technique to show the feasibility of fast measurements on aqueous polymer solutions. We have implemented the FSPN technique and a four-electrode cell with the goal of performing rapid measurements on latex suspensions. As a first test, model electrical networks which exhibit dielectric relaxation were used to demonstrate the applicability of FSPN noise generation and associated time-domain correlation techniques. However, difficulties with the signal level from our particular electronics limited the data we could obtain at this time. Thus we resorted to a sequence of single frequency measurements with the four-electrode cell on latex systems of varying size, concentration, and electrolyte concentration in order to demonstrate the feasibility of this apparatus for on-line latex size measurement.

THEORETICAL BACKGROUND

Before reviewing theoretical predictions regarding dielectric relaxation of colloidal particles, the equations which will be used to fit our experimental data in order to extract the relevant parameters for comparison with theory will be presented. For Debye single relaxation the complex dielectric constant ϵ^* is described by the Debye equation:

$$\epsilon^* = \epsilon' - j\epsilon'' = \epsilon_\infty + (\epsilon_0 - \epsilon_\infty)/[1 + j(f/f_c)] \tag{1}$$

where ϵ' and ϵ'' are the real and imaginary components of the dielectric constant, ϵ_0 is the low frequency limit of the dielectric constant, ϵ_∞ is the high frequency limit, and f_c is the central relaxation frequency.

In the case of a symmetrical distribution of relaxation times, a depressed semicircle is found for a Cole–Cole plot of ϵ' vs. ϵ''.[1,16] The Cole–Cole equation is

$$\epsilon^* = \epsilon_\infty + (\epsilon_0 - \epsilon_\infty)/\left[1 + (jf/f_c)^{(1-\alpha)}\right] \tag{2}$$

where α ranges from zero for a single relaxation to unity for an infinite distribution of relaxations. This equation is entirely empirical and reduces to the Debye equation for $\alpha = 0$.

Separating eq. (2) into real and imaginary parts gives a relationship[3,16] for the experimentally measurable quantities ϵ' and ϵ'':

$$\epsilon' = \epsilon_\infty + (\epsilon_0 - \epsilon_\infty)\left[1 + (f/f_c)^{1-\alpha}\sin(\pi\alpha/2)\right] \times \left[1 + (f/f_c)^{2(1-\alpha)} + 2(f/f_c)^{1-\alpha}\sin(\pi\alpha/2)\right]^{-1} \quad (3)$$

and

$$\epsilon'' = (\epsilon_0 - \epsilon_\infty)(f/f_c)^{1-\alpha}\cos(\pi\alpha/2) \times \left[1 + (f/f_c)^{2(1-\alpha)} + 2(f/f_c)^{1-\alpha}\sin(\pi\alpha/2)\right]^{-1} \quad (4)$$

Equations (3) and (4) reduce to the single Debye relaxation equation for $\alpha = 0$.

In practice, experimental values of ϵ' and ϵ'' obtained as a function of frequency are fitted to eqs. (3) and (4), respectively, using nonlinear regression. This gives the parameters ϵ_0, ϵ_∞, α, and f_c. In this report, ϵ_∞ was fixed at 78, which is the dielectric constant of water found at high frequency. The third method of fitting the experimental data is the "Cole–Cole fit" of ϵ'' vs. ϵ' using

$$\epsilon'' = -\epsilon_0/(2\tan^2\Phi) + 1/2\left[\epsilon_0^2/\tan^2\Phi - \epsilon_0/\tan^2\Phi + 4(\epsilon' - \epsilon_0/2)^2 - \epsilon_0^2 - \epsilon_0^2/\tan^2\Phi\right]^{1/2} \quad (5)$$

where $\Phi = (1 - \alpha)\pi/2$ and ϵ_∞ is set to zero. This equation was derived by separating eq. (2) into imaginary and real parts and eliminating the frequency terms. Equation (5) allows one to fit the data in the Cole–Cole form using nonlinear regression in order to compare with the results obtained using the ϵ' and ϵ'' data separately.

To illustrate the possible data evaluation methods, dielectric spectra are calculated using eqs. (3) and (4) and plotted in Figures 1 and 2, respectively, for $\epsilon_0 = 2000$, $\epsilon_\infty = 0$, $f_c = 1$ kHz at three different values of α; i.e., for $\alpha = 0$ (single Debye relaxation), 0.1, and 0.3. In Figure 1, the maximum at zero frequency is $\epsilon_0 = 2000$, as expected, and the frequency at half the maximum of ϵ' is the central relaxation frequency f_c and this remains constant with increasing α, although the spectrum broadens. The position of the peak in ϵ'' gives f_c in Figure 2, and the ϵ'' spectra also broadens with increasing α. The maximum value of ϵ'' at the peak is $\epsilon_0/2$ for $\alpha = 0$ and decreases significantly with increasing α.

Figure 3 contains Cole–Cole plots calculated using eq. (5) for the same α values as in Figures 1 and 2. Substantial depression of the semicircle occurs as

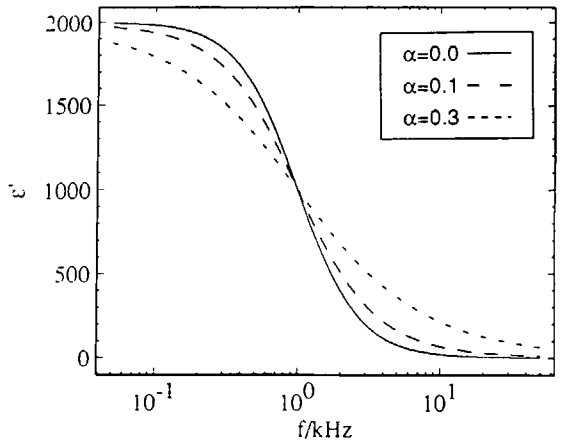

Fig. 1. Calculated values of ϵ' vs. f using $\epsilon_0 = 2000$, $f_c = 1$ kHz, and three different values of the Cole–Cole distribution parameter α indicated on the plot.

α is increased. "Graphical analysis" using the Cole–Cole equation is used as a last resort and gives a rough estimate of the experimental parameters including α.[1] To perform this analysis, the center of the depressed semicircle is determined and the angle used to determine α is calculated as indicated at the bottom of Figure 3 for the case of $\alpha = 0.3$.

Theoretical predictions of dielectric relaxation spectra from colloidal suspensions are available.[3,17-20] These are based on the assumption that counterion polarization in an oscillating electric field leads to ionic fluxes causing a huge dielectric enhancement. Consistent with the original experimental observation, the central component of most theories is that f_c is inversely proportional to the square of the particle radius.[1] Several authors have obtained explicit expression for the size dependence of f_c including Vogel and Pauly,[20]

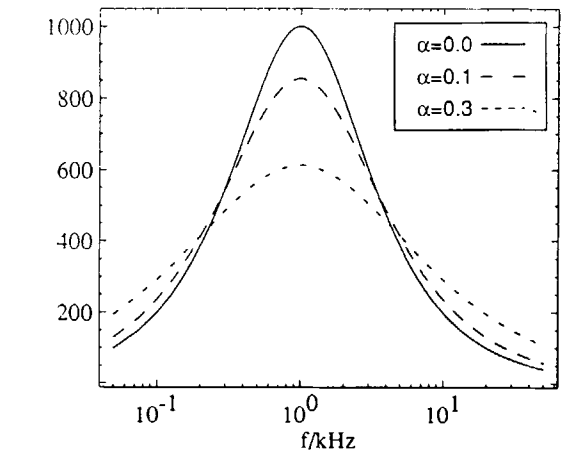

Fig. 2. Calculated values of ϵ'' vs. f using $\epsilon_0 = 2000$, $f_c = 1$ kHz, and the same values of α as in Figure 1.

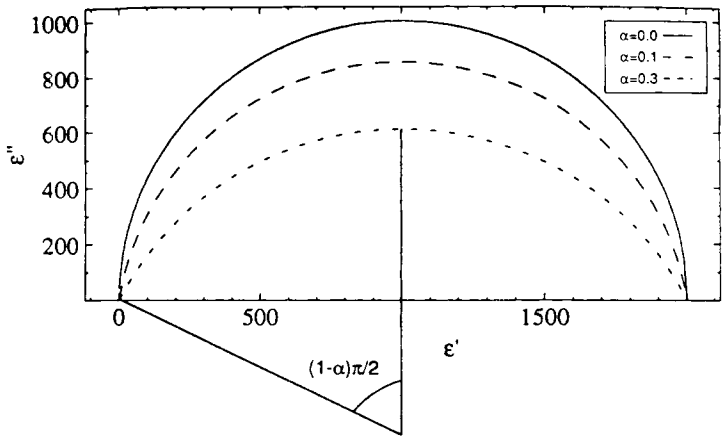

Fig. 3. Calculated Cole–Cole plots for the same parameters as in Figure 1. An example of the graphical Cole–Cole analysis is shown where $\alpha = 0.3$ is estimated from the angle determined from the depression of the semicircle as illustrated at the bottom of the figure.

who derived a rigorous expression for f_c:

$$f_c \sim 0.433D^+/(\pi a^2) \tag{6}$$

where a is the radius and $D^+ \sim 2 \times 10^{-5}$ cm^2/s is the diffusion coefficient of the counterions. The qualitative a^2 dependence is predicted by other theories,[17,18] but the proportionality constants stated in their papers are inconsistent with both experimental results and the full dielectric dispersion theory. For example, the frequency at which ϵ'' attains its maximum as predicted by the full theory (cf. Fig. 7 in deLacey and White[17]) is four times greater than that predicted by their approximate equation given by

$$f_c \sim D^+/(4\pi^2 a^2) \tag{7}$$

Also, the approximate expression

$$f_c \sim D^+/(\pi a^2) \tag{8}$$

given by Chew and Sen[18] does not agree with f_c from the peak of ϵ'' predicted from their full theory. We will discuss these predictions below, but for now it should be noted that, in order to extract reliable values of f_c, the entire theoretical dielectric dispersion calculated by these two theories must be examined, although each of these theories predicts inverse square dependence of f_c on particle diameter.

A crucial prediction of theory in terms of comparison with the results presented in this report is the breadth of the relaxation distribution. Surprisingly, all comparisons with experiment to date indicate that theory predicts spectra which are significantly broader than experiment while, intuitively, one would expect polydispersity or interparticle interactions in concentrated suspensions to have the opposite effect. In this report we have devoted significant effort to obtain statistical information on the quality of fit in terms of breadth

of the relaxation distribution characterized by α from the Cole–Cole equation. One should keep in mind that the distribution parameter α is entirely phenomenological and is only used here as a convenient parameter to compare with theory.

Theory also gives predictions of the magnitude of the dielectric constant in terms of the normalized dielectric increment defined as

$$\Delta\epsilon'/\phi = (\epsilon_0 - \epsilon_\infty)/\phi \tag{9}$$

Grosse and Foster[19] have developed a simplified theory with no adjustable parameters which scales $\Delta\epsilon'/\phi$ to the reduced quantity κa where κ is the inverse Debye screening length and a is the radius. Their results indicate that the dielectric increment $\Delta\epsilon'/\phi$ increases with κa. Theoretical results[17,19] indicate that this increase in $\Delta\epsilon'/\phi$ with κa is due to an increase of excess mobile charge in the double layer.

EXPERIMENTAL

Materials

The latex standards were obtained from Seradyne (Indianapolis, IN 46206) with a stock concentration of 10% solids and conductivities measured at 200 kHz given in Table I. All samples except the 1080 nm latex were synthesized using a persulfate initiator and an ionic surfactant such as sodium dodecyl sulfate. The 1080 nm sample was prepared with a nonionic initiator, giving it a much lower conductivity than the other samples. It was also found to be highly agglomerated as a significant fraction of solids settled to the bottom of the container within minutes of shaking. Sonication had no effect on the dielectric results for any of the samples and all samples reported here, except the 1080 nm sample, were found to be stable over a period of days.

Some samples were diluted approximately 50% with deionized water to give the needed sample volume of 25 mL. For experiments with the 721 nm latex sample where the wt % of solids was varied at constant conductivity, the suspension was successively diluted with a NaCl solution with the same conductivity to decrease the weight fraction of solids.

To perform experiments as a function of ionic strength, the 497 nm sample was dialyzed against deionized water for 20 h at room temperature and then

TABLE I
Seradyne Latex Standards, 10% Solids

Diameter (nm)	Lot #	Conductivity σ (mmho/cm)
109	LS1044E	0.89
497	1A77	0.70
721	2M4X	0.55
1080[a]	116A	0.23
1090	DL677-21	0.72

[a]Synthesized with nonionic initiator; substantial agglomeration was present.

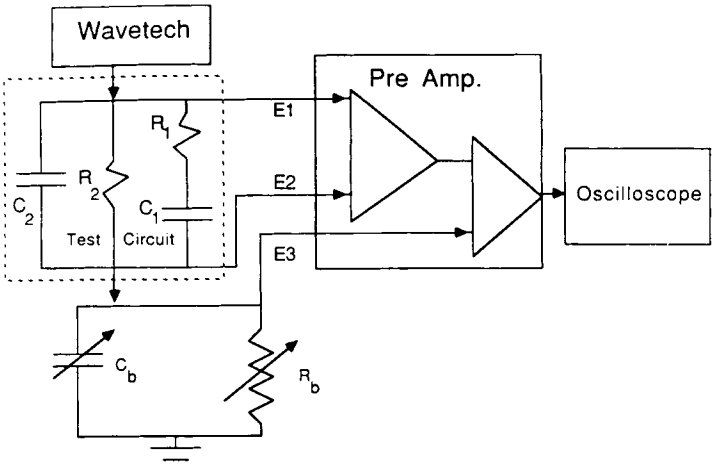

Fig. 4. Block diagram of the single frequency null-balance instrument for the test circuit. The sine wave was supplied by the Wavetech function generator and the values of R_b and C_b adjusted until zero amplitude was attained on the oscilloscope.

calculated amounts of a concentrated NaCl solution were added to successively increase the ionic strength.

Methods

Single Frequency Measurements of Model Electrical Networks

A block diagram of the setup used to perform the single frequency measurements on electrical circuits is given in Figure 4. A sine wave from the Wavetech is sent through the Debye type circuit which is comprised of R_1, C_1, R_2, and C_2, which is then connected to the preamplifier. The balance resistance R_b and capacitance C_b (General Radio 142-CB; covers the range 25–1100 pF with a precision of 0.1 pF) are adjusted for a null output on the oscilloscope at each frequency and the values of R_b and C_b are recorded.

The real and imaginary parts of the dielectric constant are related to the experimentally measured C_b and R_b by

$$\epsilon' = \theta C_b/\epsilon_p \tag{10}$$

and

$$\epsilon'' = -(1/R_{b,0} - 1/R_b)\theta/(2\pi f\epsilon_p) \tag{11}$$

where θ is the "cell" constant in cm and equal to 1 for the electrical circuits here, the permittivity constant is $\epsilon_p = 8.85 \times 10^{-14}$ F/cm and $R_{b,0}$ is the balance resistance measured at low frequency (it should approach the value of R_2 in Fig. 4).

Aqueous Latex Suspensions-Single Frequency Technique

The setup for the single frequency measurements with the latex sample cell is similar to that for the Debye circuit studies. The block diagram is given in

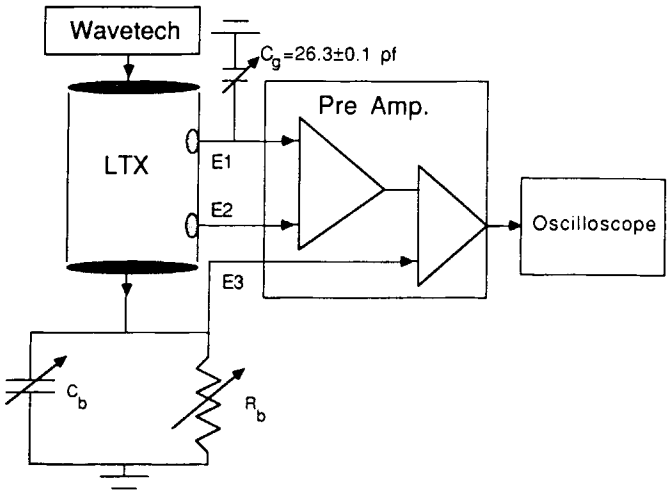

Fig. 5. Block diagram of the single frequency null-balance instrument for aqueous suspensions. The current electrodes are the dark shaded regions at the top and bottom of the four-electrode cell. The sine wave was applied to the upper current electrode and the balance circuit connected to the lower current electrode and also to E3. The potential electrodes on the side of the cell are marked by E1 and E2 and are connected to the preamplifier.

Figure 5. The signal from the wave generator s sent to the upper current electrode and the two potential electrodes, (E_1, E_2) are connected to the preamplifier. The lower current electrode is connected to the reference circuit (R_b and C_b in parallel) and to the preamplifier (E_3). R_b and C_b are adjusted at each frequency to give a null balance of the sine-wave on the oscilloscope. A detailed discussion of the modifications made to the instrument to remedy problems associated with stray capacitances will be given in the following sections.

The sample conductivity σ is related to R_b by[21]

$$\sigma = l/(R_b A) = \theta/R_b \tag{12}$$

where l is the distance between potential electrodes (~ 1.8 cm) and A is the area of the current electrodes (~ 6.7 cm^2). The ratio of l/A can be used to estimate the cell constant θ, but a more precise method to determine θ is to measure R_b for NaCl solutions of known conductivity. Our cell was found to have a constant, $\theta = 0.25 \pm 0.01$ cm^{-1}. This value was constant for all experiments presented here because the distance between potential electrodes and diameter of the current electrodes was not changed. From the measured values R_b, ϵ'' is calculated using eq. (11).

For the ideal case where no background capacitance is present, eq. (10) is used to calculate ϵ'. This equation normally has to be corrected for background capacitance as will be discussed in the context of eq. (13) below.

The single frequency experiments should be similar to those on Debye circuits in principle, but complications due to stray capacitances contributed to further difficulties. We present remedies to the three major problems which arose when we studied NaCl "blank" solutions with no latex present, yet

found R_b and C_b varied with frequency. In this test case R_b, C_b should be independent of frequency. The specific problems encountered are as follows:

1. A resistance-capacitance (RC) time constant from the electronic circuitry caused apparent dielectric relaxation in the 100–1000 kHz range due to stray capacitances.
2. A frequency independent background capacitance was detected.
3. A deviation of C_b at low frequencies was found for solutions of high conductivity.

The elimination of problem 1 above required adjustment of several experimental factors including the position of the electrodes and type of leads to the cell. The sample cell was a cylinder of 2.6 cm diameter similar to the design of Schwan and Ferris[21] with a sample volume of 25 mL. It may be seen in schematic in Figure 5. The current electrodes were 2.6 cm in diameter and the potential electrodes 0.8 cm diameter. The radial distance from the center of the cell to the potential electrodes could be varied as could the distance between current electrodes. All components were made out of Plexiglas with rubber O-rings on each electrode plug allowing the electrodes to slide freely. The electrodes were sandblasted 0.25 mm thick platinum sheet. Platinizing with platinum black[22] seemed to have negligible effect. The best results were obtained if the potential electrodes were positioned flush with the inner part of the main tubing. Schwan and Ferris[21] suggest recessing the potential electrodes to avoid stray fields but this tends to increase the resistance due to the distance from the electrical field to the recessed pickup point. We found that positioning the electrodes flush with the edge of the cell tends to reduce excess resistive impedance. This impedance accentuates the RC time constant associated with the stray capacitance in the leads of the potential electrodes.

Once the sample cell was configured to reduce the effect of resistive impedance, we turned to the problem of lead capacitances on E_1 and E_2 (Fig. 5), which also contribute to the annoying RC time constant. Coaxial cables were completely unacceptable because of their high capacitance (the BNC cables were rated at 30.8 pF/ft and BNC connectors were found to have ~ 70.5 pF each[23]), thus, low capacitance alligator clips without shielding were used. The alligator clips minimized lead capacitances but it was evident that there was still an RC time constant affecting the balance in the 100–1000 KHz region for sample resistances on the order of 3–15 kΩ.

To reduce the RC time constant further (to shift this spurious relaxation to higher frequencies where it would not affect the results), it was found that a balance of the capacitance between the leads E_1 and E_2 was necessary. Thus, a variable capacitor was connected between E_1 and ground (see Fig. 5). A value of $C_g = 26.3 \pm 0.1$ pF from E_1 to ground gave quite a flat response in terms of C_b vs. f up to $f = 1000$ kHz, although this value varies with the electronics. In Figure 6, R_b is plotted for three different values of C_g, where C_g is the value of the capacitor on E_1. It is evident that when C_g is off by only a small amount, R_b tails upward or downward at high frequencies. If C_g is too low, R_b decreases and if C_g is too high, R_b increases. The balance capacitance C_b is not as sensitive but also can be seen to change by a few picofarads at high frequencies if C_g is not 26.3 ± 0.1 pF. The remaining RC time constant is

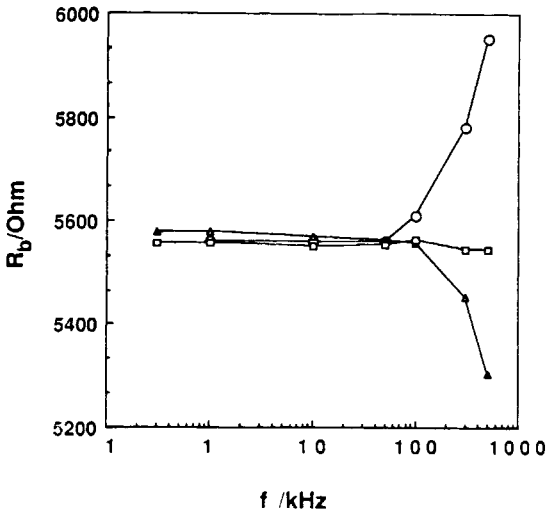

Fig. 6. Single frequency measurements of the balance resistance R_b vs. f for a 0.5 mM NaCl "blank" solution. Three values of the lead capacitance C_g (see Fig. 5) were chosen including 28 pF (○), to 26.3 pF (□), and 23 pF (▲). The desired response is the flat response seen for C_g = 26.3 pF.

shifted to higher frequencies if the sample conductivity is increased (i.e., the sample resistance is decreased) as is expected. This is because the stray capacitance C_s, contributing to a RC time constant, is at an approximate frequency $f_s \sim 1/(2\pi R_b C_s)$, where R_b is related to the conductivity of the solution.

Problem 2 is a minor one because it is a frequency-independent contribution to the measured C_b and can be easily compensated. Assuming $\epsilon' = 78$ which is the static dielectric constant of water, then $C_{b,\,\text{ideal}}$ for water according to eq. (10) is

$$C_{b,\text{ideal}} = (8.85 \times 10^{-14}\text{F/cm}) \times 78/0.25\ \text{cm}^{-1} = 27.6\ \text{pF} \qquad (13)$$

A typical measured value for C_b at high frequencies ($\sim$ 500 kHz) is say 50 pF, giving a value for the background capacitance of 50 − 27.6 = 22.4 pF. Thus all measured values of C_b are corrected by subtracting the background capacitance so that

$$\epsilon' = \theta(C_b - 22.4\ \text{pF})/\epsilon_p \qquad (14)$$

The background capacitance generally depends on the length of the BNC cables connecting the cell to the reference circuit and also the wiring in the reference circuit itself. With a given instrument configuration this calibration is good for months and all subsequent data can easily be normalized to $\epsilon' = 78$ at high frequencies.

Problem 3 was encountered with highly conductive solutions at low frequencies. When working with high concentration NaCl blank solutions, it was found that C_b drifted upward or downward at low frequencies and this effect was magnified as the conductivity increased, even though C_b was independent

of conductivity at high frequencies. There was no variation in R_b within experimental error. Surprisingly the direction of the change in C_b could be reversed by adjusting the current electrodes. By trial and error adjustment it was possible to get a relatively flat response of C_b with frequency. Unfortunately, this was rather difficult, so periodically a blank experiment was performed with a NaCl solution with the same conductivity and the excess capacitance was subtracted. A permanent solution to this problem is being sought through an improved cell design.

Fourier Synthesized Pseudo Random Noise (FSPN) Method

It has been shown that white noise with a flat power spectrum as the impulse excitation has advantages over pulse type excitations.[15] Following Nakamura et al.,[15] we have digitally generated Fourier synthesized pseudo random white noise $f(t)$ using the random phase approximation:

$$f(t) = \sum A_k \exp[j(\omega_k t + \Phi_k)] \tag{15}$$

where Φ_k is a random number between 0 and 2π. Approximately 512 frequencies ω_k were used and the amplitude function A_k was set equal to unity.[15] Examination of the power spectrum of the white noise using a Nicolet 444A spectrum analyzer indicated that the power was constant over at least 2 orders of magnitude in frequency. Seven different frequency ranges starting from approximately 60 Hz and ending at 2 MHz could be programmed depending on the frequency range of interest.

The block diagram of the FSPN instrument for the latex sample cell is given in Figure 7. The voltage to current (V/I) converter is used to process the input white noise to the cell and operational amplifiers, while A/D converters

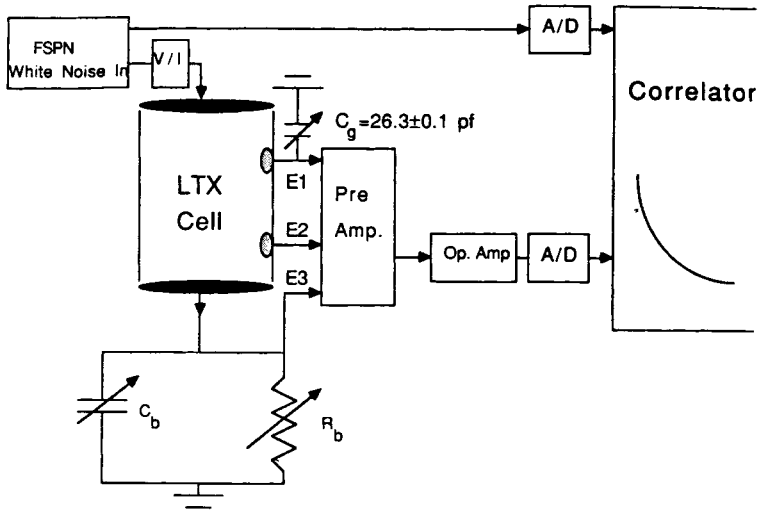

Fig. 7. Block diagram of the FSPN instrument for latex samples. The setup is the same as that shown in Figure 5 except the input signal is processed by a voltage to current convertor V/I and the detection scheme consists of A/D converters and a Malvern correlator.

are used to process the output signals to the correlator (Malvern K7025). The A/D conversion is done by a dual voltage-to-light (V/L) converter (RR131, Malvern Instruments, Malvern, U.K.), which consists of two light emitting lamps and two photon-counting photomultiplier tubes with associated discriminator electronics. The output of the preamplifier is amplified with a high speed op-amp to improve signal-to-noise. Amplification is difficult because the V/L has a 50 Ω input impedance, limiting the sensitivity of the measurement. Unfortunately, this problem with our electronics limited the range of data we could take using the FSPN technique for latex samples. For the electronic circuit tests the same configuration as in Figure 7 is used except the sample cell is replaced by a test circuit such as that in Figure 4. In this case the operational amplifier on the "pre-amp out" is not needed because the signal is made sufficiently strong by choosing proper values of R_2.

For a system exhibiting dielectric relaxation as in eq. (1), the cross-correlation function on the correlator can be represented by an exponentially decaying function in the time domain[24, 25]:

$$g(t) \sim [1 - \exp(-t/\tau_0)] \tag{16}$$

where the relaxation time is related to the central relaxation frequency f_c by

$$\tau_0 = 1/(2\pi f_c) \tag{17}$$

This allows comparison of the FSPN and single frequency methods.

RESULTS AND DISCUSSION

Tests with Debye Electronic Circuits

Single Frequency Measurements

An essential test of both the single frequency and FSPN dielectric instruments is the analysis of an idealized sample cell which can be simulated using resistors and capacitors. The circuit components used to construct a Debye type circuit are shown in Figure 4 and Table II. These were chosen to cover a

TABLE II
Summary of Results for Test Circuits[a]

R_1 (Ω)	Theoretical $f_c = 1/(2\pi R_1 C_1)$ (Hz)	Experimental f_c(single freq.) (Hz)	Experimental f_c(FSPN) (Hz)
3918	24,000	23,000	12,000
21,700	4350	4200	3500
57,400	1640	1500	1365
219,000	430	400	403

[a] C_1 = 1690 pF, R_2 = 8000 Ω, and C_2 = 100 pF for all these circuits.

wide range of central relaxation frequencies defined theoretically by

$$f_c = 1/(2\pi R_1 C_1) \tag{18}$$

As was discussed above, the experimental data can be fitted by nonlinear regression to three different variations of the Cole–Cole equation [eqs. (3), (4), and (5) corresponding to ϵ', ϵ'', and Cole–Cole fits, respectively], all of which should give the same result. The results are summarized in Table II in terms of f_c (single freq.) showing good agreement with theoretical values predicted by eq. (18) for the test circuits for a range of values of f_c. To illustrate the consistency of the results, the nonlinear regression results on the first test circuit with $R_1 = 3918\ \Omega$ give (for ϵ', ϵ'', and Cole–Cole fits, respectively) values of f_c of 23.1 ± 0.3, 22.8 ± 0.1, and 23.0 ± 0.1 kHz; values of ϵ_0 of $19{,}600 \pm 100$, $20{,}000 \pm 70$, and $19{,}700 \pm 100$; and values of α of 0.002, 0.012, and 0.001. These values of α are zero within experimental error and reflect an ideal, narrow Debye distribution of relaxation times as would be expected for this model circuit. For this data the three modes of fitting the experimental data are equivalent.

FSPN Measurements on Debye Circuits

The FSPN schematic, shown in Figure 7, was tested using the test circuits in place of the latex cell. The circuit was balanced for a null output at high frequencies ($\sim$ 300 kHz) before taking the cross-correlation function. The cross-correlation function was fitted to an exponential relaxation time constant τ_0, and the values are listed in Table II. To illustrate the range of agreement with theory, the value of $1/f_c$, from Table II is plotted vs. R_1 in Figure 8 for both single frequency and FSPN techniques. This should yield a straight line since C_1 was kept constant in these experiments. A significant deviation in f_c(FSPN) with increasing frequency is seen starting at about 5000 Hz. This is due to the high frequency drop-off in performance of our V/l converter. In our present electronics, the load R_2 across the circuit is made

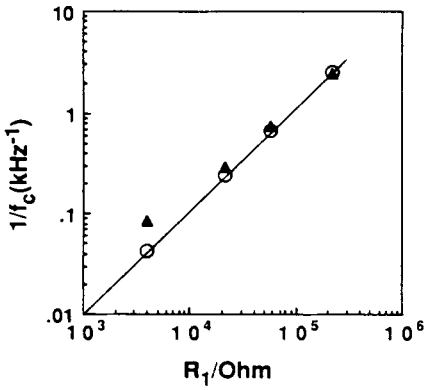

Fig. 8. Reciprocal f_c vs. R_1 for the single frequency (○) and FSPN (▲) measurements. The FSPN results deviate from the predicted inverse proportionality at high frequencies while the single frequency results agree over the whole range.

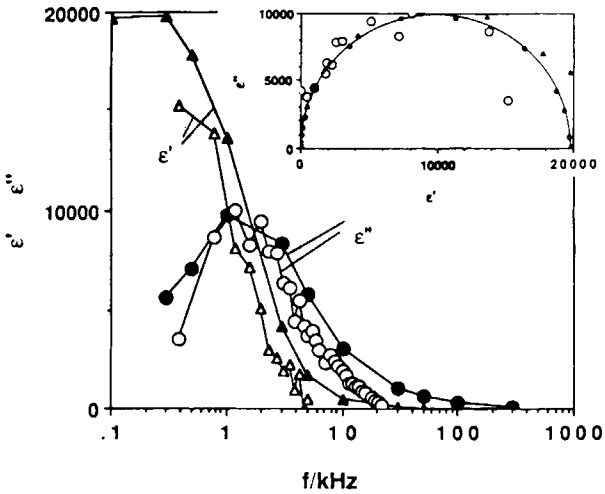

Fig. 9. Real dielectric constant ϵ' and imaginary dielectric constant ϵ'' for FSPN (open symbols) and single frequency (filled symbols) for a test circuit with $R_1 = 57.4$ kΩ, $C_1 = 1690$ pf, $R_2 = 8.0$ kΩ, and $C_2 = 100$ pf. The inset is a Cole–Cole plot of the FSPN results for $R_1 = 57.4$ kΩ (○) along with single frequency measurements for $R_1 = 57.4$ kΩ (●) and $R_1 = 3.918$ kΩ (▲) at the same values of C_1, R_2, and C_2 as above. All results superimpose onto a semicircle with $\alpha = 0$, although there is some scatter for the FSPN data.

rather large in order to get a sufficiently strong signal, and the electronics fail at high frequencies for such large voltages. About half a decade in frequency on either side of f_c is necessary for its determination so we conclude that, with our electronics, the FSPN technique is relatively accurate in the range 50–10,000 Hz. The single frequency measurements are accurate over the whole range in Figure 8 because the V/I converter is not used. We found the measurable range to be about 20 Hz to over 1 MHz for these electrical circuits.

To compare the FSPN and single frequency techniques in terms of the detailed frequency response, the cross-correlation function results were transformed using the fast Fourier transform from time to frequency domain. The values of ϵ' and ϵ'' obtained were scaled by a factor of 338 to take into account the gain and other instrument constants[15] and are plotted in Figure 9 together with the single frequency results. The inset of Figure 9 is a Cole–Cole plot of the FSPN measurements and the single frequency measurements. All the single frequency Cole–Cole plot results are independent of R_1 and form a semicircle even though f_c itself varies with R_1. The semicircular nature of the Cole–Cole plot with $\alpha \sim 0 \pm 0.001$ is indicative of a Debye single relaxation. The FSPN results in the inset also superimpose on this semicircle, although there is more scatter.

Latex Measurements

Single Frequency Measurements

The experimental apparatus shown in Figure 5 was used to determine the dielectric response of polymer latex samples. The results will be discussed in subsequent sections.

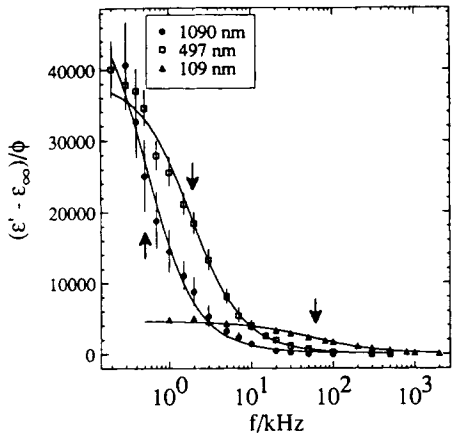

Fig. 10. Real part of the dielectric constant $(\epsilon' - \epsilon_\infty)/\phi$ vs. f (i.e., normalized by the weight fraction ϕ with $\epsilon_\infty = 78$) for latex standards with diameters indicated in the legend. The arrows indicate the central relaxation frequencies for each particle size. The solid curves are fits to the Cole–Cole equation.

Particle Size Dependence. The dielectric frequency response for Dow latex standards with diameters of 109, 497, and 1090 nm are plotted in Figures 10 and 11 along with best fits obtained using nonlinear regression. The data was weighted inversely proportional to the error bars shown. The real part ϵ' in Figure 10 has been normalized and plotted as $(\epsilon' - \epsilon_\infty)/\phi$ in order to facilitate comparison of absolute magnitudes, where ϕ is the wt % solids and $\epsilon_\infty = 78$ is the dielectric constant of water. The imaginary part ϵ'' in Figure 11 is also normalized by dividing by ϕ. The results for the 721 nm standard are omitted to avoid confusion due to the overlapping of the data and these results are included in the summary in Table III and plotted in Figures 12 and 13.

Regression fits to the data give the three parameters f_c, α, and ϵ_0. The values of f_c determined for the 497, 721, and 1090 nm standards using the

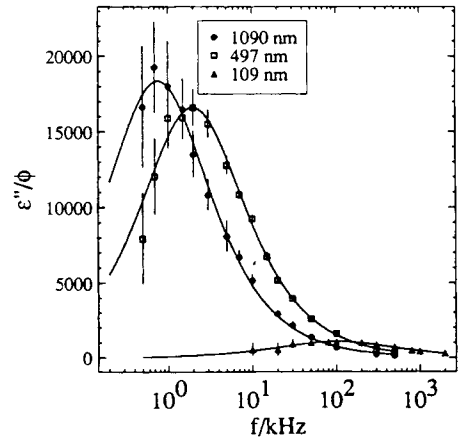

Fig. 11. Imaginary dielectric loss ϵ''/ϕ normalized by the weight fraction ϕ vs. f for the same latex standards as in Figure 10. The solid curves are fits to the Cole–Cole equation.

TABLE III
Dielectric Results for Latex Standards

d (nm)	Regression method	% Solids	σ (mmho/cm)	κa	α	$\Delta\epsilon'/\phi$ ($\times 10^{-3}$)	f_c (kHz)
109	ϵ'	10	0.89	18.1	0.27 ± 0.04	4.6 ± 0.2	56 ± 7
	ϵ''				0.25 ± 0.1	3.2 ± .4	100 ± 26
	Cole–Cole				0.34[b]	4.9[b]	80[b]
497	ϵ'	4	0.28	46.2	0.15 ± 0.01	39 ± 3	1.85 ± 0.2
	ϵ''				0.16 ± 0.01	43 ± 2	2.0 ± 0.1
	Cole–Cole				0.12 ± 0.01	40 ± 2	2.0 ± 0.1
721	ϵ'	6	0.33	72.8	0.09 ± 0.005	55 ± 3	1.22 ± 0.1
	ϵ''				0.1 ± 0.01	63 ± 2	1.06 ± 0.05
	Cole–Cole				0.08 ± 0.005	56 ± 2	1.2 ± .1
1080[a]	ϵ'	6	0.14	71.0	0.05 ± 0.005	163 ± 8	0.2 ± 0.01
	ϵ''				0.05 ± 0.02	104 ± 5	0.24 ± 0.02
	Cole–Cole				0.08 ± .03	119 ± 10	0.27 ± 0.03
1090	ϵ'	6	0.43	125.6	0.13 ± 0.02	52 ± 10	0.54 ± 0.1
	ϵ''				0.15 ± 0.02	47 ± 10	0.76 ± 0.2
	Cole–Cole				0.08[b]	37[b]	0.52[b]

[a] This sample was agglomerated and the results are not plotted in Figure 10.
[b] Fitting using nonlinear regression of the data with the Cole–Cole analysis was not possible because the semicircle was deformed significantly. Approximate results from the graphical Cole–Cole method are given instead.

three different fitting methods are consistent within experimental error determined from the covariance matrix. We feel that the raw ϵ' data is the most accurate so these fitting results are possibly more reliable. The Cole–Cole fit [eq. (5)] is a two parameter regression fit giving only ϵ_0 and α. The third parameter, f_c, is found by examining the data and choosing the frequency corresponding to the apex of the semicircle.

The results for the smallest diameter latex were not consistent with the other samples in many aspects. The peak in ϵ'' corresponded to $f_c = 100 \pm 26$ kHz (Fig. 11) while, for ϵ', $f_c = 56 \pm 7$ kHz (Fig. 10). The values of ϵ'' are very

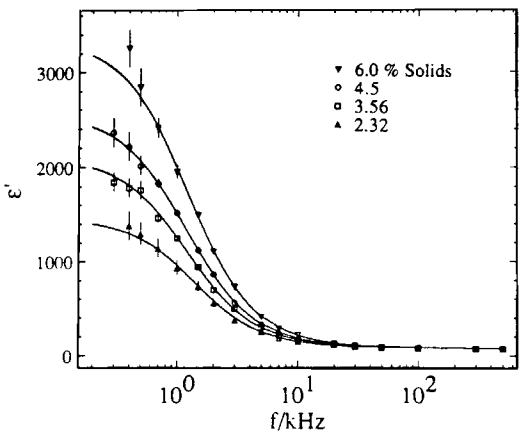

Fig. 12. Real dielectric constant ϵ' vs. f for the $d = 721$ nm latex standard at the weight fractions indicated. The solid curves are fits to the Cole–Cole equation.

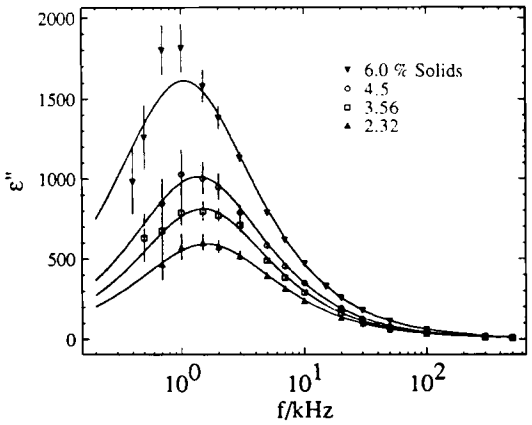

Fig. 13. Imaginary dielectric constant ϵ'' vs. f for the 721 nm standard at the weight fractions indicated. The solid curves are fits to the Cole–Cole equation.

small and are not reliable because of conductivity drifts which is possibly why the critical frequencies do not agree. The values of α were also significantly higher than for the other samples.

The values of ϵ_0 are reported as a dielectric increment defined as $\Delta\epsilon'/\phi = (\epsilon_0 - \epsilon_\infty)/\phi$, which allows comparison of absolute magnitudes. It is evident that $\Delta\epsilon'/\phi$ generally increases with diameter in Table III.

In some cases the graphical Cole–Cole analysis[1,16] was used instead of fitting directly to the Cole–Cole equation (5). These results are reported in Table III for the 109 and 1090 nm samples and are considered "lower quality" because of inaccuracy in ϵ''. The results for the 1080 nm sample deviated systematically giving small values of f_c, indicating larger apparent particle sizes due to aggregation as was discussed previously. Surprisingly enough, the fits of ϵ' and ϵ'' for the 1080 nm sample to eqs. (3) and (4), respectively, were quite good for this agglomerated latex. The small values of α indicate a narrow distribution of relaxation times. The aggregates are quite large, causing an increase in the values of ϵ' at low frequencies (note that in Table III $\Delta\epsilon'/\phi$ is very large), without really changing the shape of the curve at higher frequencies, giving rise to an apparently narrow distribution. Still, f_c is shifted to smaller values because of the larger ϵ_0.

Solids Concentration Dependence. The real and imaginary dielectric constants are plotted in Figures 12 and 13, respectively, for wt % solids from 2.32% to 6.0% of the 721 nm standard, showing a strong dependence of magnitude on concentration. Scaling by dividing by the volume fraction reduces the data into one set, as was reported previously,[7,10,11] as indicated by the dielectric increment $\Delta\epsilon'/\phi = (\epsilon_0 - \epsilon_\infty)/\phi$ reported in Table IV. The values of f_c and α are listed in Table IV and are also constant within experimental error with no difference in parameters obtained from the nonlinear regression fits to the ϵ', ϵ'', and Cole–Cole data. A representative Cole–Cole plot for 4.5% solids is given in Figure 14 along with the fit to eq. (5). It is evident that the data agree well, especially in the high frequency region on the left-hand side of the plot.

TABLE IV
Weight Fraction Dependence, 721 nm Latex[a]

% Solids	Regression method	α	$\Delta\epsilon'/\phi$ ($\times 10^{-3}$)	f_c (kHz)
2.32	ϵ'	0.1 ± 0.01	61 ± 6	1.4 ± 0.2
	ϵ''	0.11 ± 0.02	62 ± 4	1.6 ± 0.2
	Cole–Cole	0.06 ± 0.005	55 ± 3	1.4 ± 0.2
3.56	ϵ'	0.1 ± 0.01	58 ± 3	1.2 ± 0.1
	ϵ''	0.08 ± 0.01	52 ± 2	1.4 ± 0.1
	Cole–Cole	0.09 ± 0.01	54 ± 2	1.4 ± 0.2
4.5	ϵ'	0.1 ± 0.006	56 ± 2	1.2 ± 0.06
	ϵ''	0.09 ± 0.02	51 ± 4	1.4 ± 0.1
	Cole–Cole	0.09 ± 0.005	51 ± 5	1.3 ± 0.1
6.0	ϵ'	0.09 ± 0.005	55 ± 3	1.2 ± 0.1
	ϵ''	0.1 ± 0.01	63 ± 2	1.06 ± 0.05
	Cole–Cole	0.08 ± 0.05	57 ± 2	1.2 ± 0.1

[a] $\kappa a = 74$, 3.4 mM NaCl.

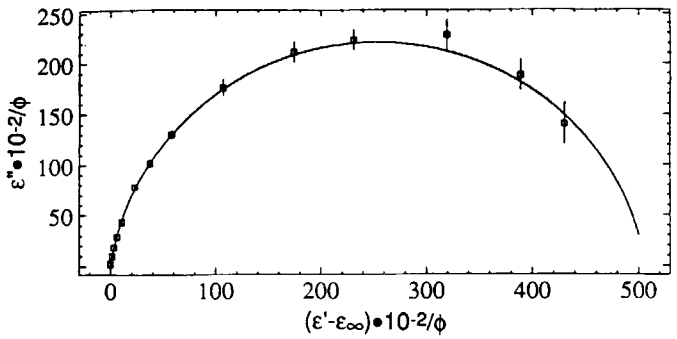

Fig. 14. Cole–Cole plots of the imaginary ϵ''/ϕ vs. the real $(\epsilon' - \epsilon_\infty)/\phi$ dielectric constants normalized to the volume fraction ϕ for the 721 nm latex standard at a weight fraction of 4.5%.

Ionic Strength Dependence. After dialysis, successive amounts of a concentrated NaCl solution were added to increase the ionic strength of the 497 nm latex suspension. The values of κa in Table V were calculated assuming a monovalent electrolyte. For the lowest conductivity solution the electrolytic species is not known because of the dialysis procedure. Dialysis seemed to change the latex surface properties slightly[3] because f_c increased from 2 kHz (cf. Table III) before dialysis to around 4 ± 1 kHz after dialysis, independent of conductivity. Cole–Cole fits were made using the graphical method and the results are shown in Figure 15. Regression fits of the separate ϵ' and ϵ'' data

TABLE V
Ionic Strength Dependence 497 nm Latex at 4% Solids

σ (mmho/cm)	κa	α	$\Delta\epsilon'/\phi$	f_c (kHz)
0.04	17.5	0.40 ± 0.08	10,300	3 ± 1
0.14	32.7	0.28 ± 0.08	17,300	5 ± 1
0.31	48.6	0.03 ± 0.05	22,100	4.5 ± 1

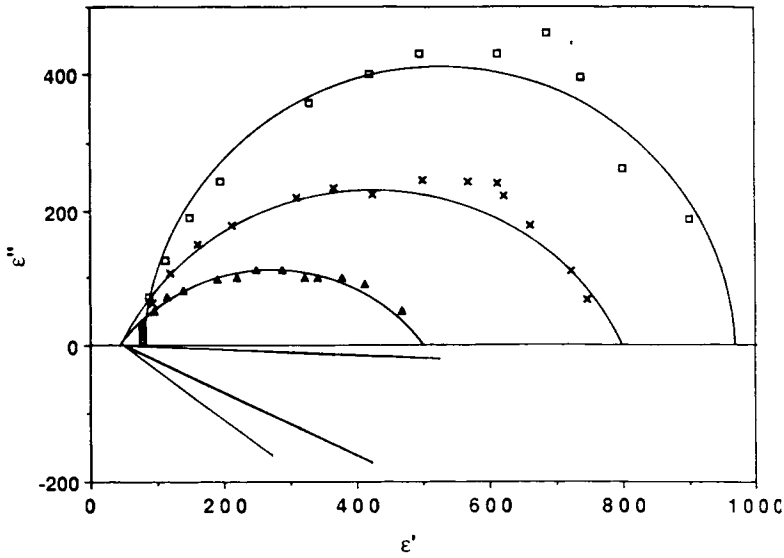

Fig. 15. Cole–Cole plots of ϵ'' vs. ϵ' for the d = 497 nm standard at a weight fraction of 4% and conductivities of 0.04 mmho/cm (▲), 0.14 mmho/cm (×), and 0.31 mmho/cm (□).

were not successful due to the poor quality of the data. The results of the graphical fits in Table V indicate that while f_c remains relatively constant, as was seen previously,[3,6] $\Delta\epsilon'/\phi$ and α are strongly dependent on conductivity[3,6] with α increasing with decreasing ionic strength, indicating a broader distribution of relaxations. The magnitude of the dielectric increment $\Delta\epsilon'/\phi$ increases substantially with ionic strength. This will be discussed in more detail in the next section.

Discussion of Single Frequency Latex Results

Central Relaxation Frequency f_c. Experimental and predicted values of f_c from the literature and this report are plotted vs. diameter in Figure 16, indicating our results are essentially identical to those of Schwan et al.[1], who covered a large range of particle sizes and took care to prevent agglomeration. One experimental data point deviates from the rest.[10] Amphoteric latex was studied in this case under conditions where the fixed surface charge was positive while all other reported samples had negative surface charges. Whether the positive charge contributes to a shift in f_c to lower values is not known. Theoretical predictions of f_c taken from Figure 7 of deLacey and White,[17] Figure 4 of Chew and Sen,[18] and Figure 3 of Grosse and Foster,[19] and the expression given as eq. (6) in this report, derived by Vogel and Pauly,[20] are also plotted in Figure 16. All of the theories can be represented by the solid line in Figure 16 because they all lead to $1/a^2$ dependence of f_c and yield essentially the same predictions over the particle range studied. Reasonable agreement with experiment is seen between experiment and theory for both the slope ($1/a^2$ dependence) and absolute magnitude of f_c (within 30%).

Breadth of Dielectric Relaxation. Another important experimental variable is the breadth of the distribution of relaxation frequencies characterized

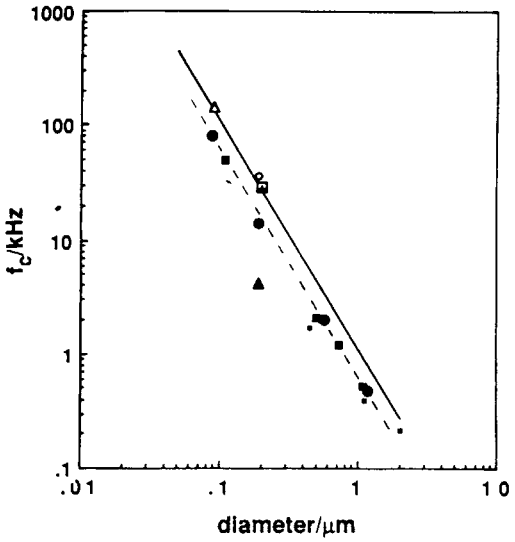

Fig. 16. Central relaxation frequency f_c vs. diameter for experimental data from this report (■), Schwan et al.[1] (●), Ballario et al.[2] (△), Lim and Franses[7] (▪), and Myers[10] (▲). Theoretical results are from Vogel and Pauly[20] (△), deLacey and White[17] (□), Chew and Sen[18] (○), and Grosse and Foster[19] (+). All the theoretical predictions may be represented by the solid line. The dashed line is drawn through the experimental data of Schwan et al.[1]

by α. Values of α are close to 0.12 ± 0.03 (Tables III and IV) for the $d = 497$, 721, and 1090 nm samples, irrespective of the method of fitting and increase to 0.27 ± 0.04 for the 109 nm sample. Lim and Franses[7] also reported small α values between 0.02 and 0.1 for a $d = 2000$ nm latex sample, Bellario et al.[2-3] reported $\alpha = 0.15$ for $d = 91$ nm, Springer et al.[6] reported $\alpha = 0.15$ for $d = 444$ nm and stated that it decreased as the conductivity was increased. For smaller diameter standards, α increased to values greater than 0.15.[1,3,7]

A Cole–Cole analysis of the theoretical predictions of deLacey and White[17] indicate that α is a strong function of κa. Simulations of the theoretical equations of deLacy and White for three particle diameters were carried out and the resulting "data" analysed for f_c, and α. By performing nonlinear regression on the values of ϵ'' via eq. (4) for three diameters including $d = 229$ nm ($\kappa a = 13$), $d = 416$ nm ($\kappa a = 23$), and $d = 1000$ nm ($\kappa a = 56$), gives $\alpha = 0.34$, $\alpha = 0.21$, and $\alpha = 0.14$, respectively. The agreement of the value of α found with the experimental trend in Table III as a function of κa is remarkable and to our knowledge this point has not been discussed before in terms of the breadth of the relaxation as predicted by theory. The theoretical spectra are not completely symmetric and the fit to ϵ' is slightly worse than the fit to ϵ'' discussed above.

Grosse and Foster[19] report that the best fit to their theory gives $\alpha = 0.42$ and is independent of κa. Vogel and Pauly[20] have considered higher order terms in the density expansion for relatively large values of κa. Reanalyzing results in Figure 3 of their paper by the graphical Cole–Cole method indicates that including these terms lowers α roughly from 0.33 to 0.19 by diminishing the low frequency tail which occurs at large scales of ϵ'. The Cole–Cole equation does not fit their predictions well because of a slight lack of

symmetry at all frequencies.[20] Values of α tending towards zero are obtained (i.e., $0.0 < \alpha < 0.2$) if one disregards the low frequency tails in their Cole–Cole plots. On the other hand, experiment agrees exceedingly well with the Cole–Cole equation (see Fig. 14 and Ref. 6) especially in the high frequency region.

Coming to the ionic strength data obtained for the 497 nm standard (Table V), the trend was that α increased as the ionic strength was lowered, as was reported previously.[6,7] This is also consistent with an increase in κa, leading to a decrease in α.

Dielectric Increment, $\Delta\epsilon'/\phi$. Grosse and Foster[19] have developed a simplified theory with no adjustable parameters which scales $\Delta\epsilon'/\phi$ and f_c to the reduced quantity κa, where κ is the inverse Debye screening length and a is the latex radius. They have shown good agreement between their predictions of $\Delta\epsilon'/\phi$ and experiment. Our data (Tables III–IV) also show good agreement with their predictions, but our results are generally 10–40% lower in magnitude, except for the 1090 nm standard which is almost an order of magnitude lower.

Several rigorous theories are available which take into account the effect of the surface zeta potential ζ.[17,18,20] This is a measurable quantity but the values experimentally determined are much lower than the values needed to theoretically fit experimental data for the dielectric increment.[10,12] Another inconsistency arises because an increase in ζ would also theoretically produce an increase in $\Delta\epsilon'/\phi$.[17,18] However, experimental determination of ζ[26,27] indicates that it is strongly dependent on the particle size and ionic strength, and actually decreases with increasing ionic strength. This is in contradiction to experimental results[6,7] including our own, which indicate that $\Delta\epsilon'/\phi$ increases with ionic strength. Thus, the decrease in excess mobile charge in the double layer,[17] as the ionic strength increases (or κa decreases), causes $\Delta\epsilon'/\phi$ to decrease and this effect dominates any influence of the zeta potential, ζ.[5]

FSPN Measurements

Figure 7 is the block diagram of the instrument used for the FSPN measurements. Because the measurement is a differential one, the cell is balanced a high frequencies ($\sim$ 300 kHz) before taking the cross-correlation function. The signal is generally weak and the voltage is controlled by the sample conductivity, with higher conductivities giving lower voltages. FSPN experiments on the latex samples were not successful because dielectric measurements are inherently insensitive at low frequencies, a small change in sample capacitance at low frequencies leads to an imperceptible change in signal voltage. Because of the limitation in our electronics, the voltage to light converter, which acts as an A/D converter, is not sensitive to amplitudes less than $\sim$ 10 mV, leading to a flat voltage response at low frequencies and almost no correlation. Efforts to boost this signal with a heavier load on the cell gave poor performance at high frequencies. Thus we cannot report consistent results with the FSPN technique at this time. Improvements in the FSPN electronics are progressing and the results will appear in a forthcoming paper.

Summary of Latex Results

Using a four-electrode cell to avoid electrode polarization, single frequency measurements were performed in the range 0.05 kHz $< f <$ 500 kHz on latex standards of varying size, latex concentration, and electrolyte concentration. Our data taken for 2–10% solids was in agreement with previous results obtained at concentrations up to 30%, indicating that the central relaxation frequency f_c is inversely proportional to the square of the diameter. The absolute magnitude of the dielectric constant as a function of size, volume fraction, and ionic strength was found to agree with the theory of Grosse and Foster.[19] An important experimental variable affecting the distribution of dielectric relaxation times is the inverse screening length κ times the particle radius a. For the higher κa values, Cole–Cole distribution parameters determined from nonlinear regression fits were relatively narrow ($\alpha = 0.15 \pm 0.02$, $\alpha = 0.09 \pm 0.01$, and $\alpha = 0.13 \pm 0.04$, for $d = 497$ nm ($\kappa a = 46.2$), $d = 721$ nm ($\kappa a = 72.8$), and $d = 1090$ nm ($\kappa a = 125.6$) latex standards, respectively). The relaxation distribution increased substantially to $\alpha = 0.27 \pm 0.04$ for the 109 nm latex standard ($\kappa a = 18.1$). Analysis of α from ϵ'' predictions generated by the theory of deLacy and White[17] gave $\alpha = 0.34$, $\alpha = 0.21$, and $\alpha = 0.14$, for $d = 229$ nm ($\kappa a = 13$), $d = 416$ nm ($\kappa a = 23$), and $d = 1000$ nm ($\kappa a = 56$), respectively. These results qualitatively explain the trend in the experimental data with the distribution narrowing significantly at higher values of κa. The variation from $\alpha = 0.4 \pm 0.08$ ($\kappa a = 17.5$) at low ionic strength to $\alpha = 0.03 \pm 0.05$ ($\kappa a = 48.6$) at higher ionic strength for the 497 nm latex standard again supports the trend of decreasing α with increas ing κa.

The results of this work demonstrate the feasibility of dielectric spectroscopy as a rapid analysis tool for particle size determination in polymer latices. The single frequency method requires 5–10 min per measurement while the FSPN technique requires only a few seconds. Both methods are amenable to on-line measurement. Experiments applying this instrument to experimental reactors on-line are in progress.

We would like to gratefully acknowledge the support of the National Science Foundation and the industrial sponsors of the University of Wisconsin Polymerization Reaction Engineering Laboratory (UWPREL). We also thank D. F. Myers and D. A. Saville for sending us preprints of their work. We are grateful to L. Rosen for providing predictions from the theory of deLacy and White and for critical comments on the manuscript.

References

1. H. P. Schwan, G. Schwartz, J. Maczuk, and H. Pauly, *J. Phys. Chem.*, **66**, 2626 (1962).
2. C. Ballario, A. Bonincontro, and C. Cametti, *J. Colloid Interface Sci.*, **54**, 415 (1976).
3. C. Ballario, A. Bonincontro, and C. Cametti, *J. Colloid Interface Sci.*, **72**, 304 (1979).
4. M. M. Springer, Ph.D. thesis, University of Wageningen, Denmark, 1979.
5. S. Sasaki, A. Ishikawa, and T. Hanai, *Biophys. Chem.*, **14**, 45 (1981).
6. M. M. Springer, A. Korteweg, and J. Lyklema *J. Electroanal. Chem.*, **153**, 55 (1983).
7. K. -H. Lim and E. I. Franses, *J. Colloid Interface Sci.*, **110**, 201 (1986).
8. R. Hayakawa, H. Kanda, M. Sakamoto, and Y. Wada, *Jpn. J. Appl. Phys.*, **14**, 2039 (1975).
9. S. Umemura, R. Hayakawa, and Y. Wada, *Biophys. Chem.*, **11**, 317 (1980).
10. D. F. Myers, Ph.D. thesis, Princeton University, 1988.

11. D. F. Myers and D. A. Saville, *J. Colloid Interface Sci.*, **131**, 448 (1989).
12. D. F. Myers and D. A. Saville, *J. Colloid Interface Sci.*, **131**, 461 (1989).
13. Y. Husimi and A. Wada, *Rev. Sci. Instrum.*, **47**, 213 (1976).
14. Y. Husimi, H. Nakamura, and A. Wada, *Ann. N.Y. Acad. Sci.*, **303**, 90 (1977).
15. H. Nakamura, Y. Husimi, and A. Wada, *J. Appl. Phys.*, **52**, 3053 (1981).
16. K. S. Cole and R. H. Cole, *J. Chem. Phys.*, **9**, 341 (1941).
17. E. H. B. deLacey and L. R. White, *Chem. Soc., Faraday Trans.* 2, **77**, 2007 (1981).
18. W. C. Chew and P. N. Sen, *J. Chem. Phys.*, **77**, 4683 (1982).
19. C. Grosse and K. R. Foster, *J. Phys. Chem.*, **91**, 3073 (1987).
20. E. Vogel and H. Pauly, *J. Chem. Phys.*, **89**, 3823, 3830 (1988).
21. H. P. Schwan and C. D. Ferris, *Rev. Sci. Instrum.*, **39**, 481 (1968).
22. H. P. Schwan in, *Physical Techniques in Biological Research*, W. L. Nastuk, Ed., Academic, New York, 1963, Vol VI.
23. R. S. Stock, Ph.D. thesis, University of Wisconsin-Madison, 1986.
24. M. J. C. van Gemert, *J. Chem. Phys.*, **60**, 3963 (1974).
25. R. H. Cole, *J. Phys. Chem.*, **79**, 1459 (1975).
26. R. H. Ottewill and J. N. Shaw, *Discuss Faraday Soc.*, **42**, 154 (1966).
27. R. H. Ottewill and J. N. Shaw, *J. Electroanal. Chem.*, **37**, 133 (1972).

Received July 14, 1989
Accepted January 2, 1990